Response of the North Atlantic Thermohaline Circulation and Ventilation to Increasing Carbon Dioxide in CCSM3

FRANK O. BRYAN AND GOKHAN DANABASOGLU

National Center for Atmospheric Research, Boulder, Colorado*

NORIKAZU NAKASHIKI, YOSHIKATSU YOSHIDA, DONG-HOON KIM, AND JUNICHI TSUTSUI

Central Research Institute of Electric Power Industry, Abiko, Japan

SCOTT C. DONEY

Woods Hole Oceanographic Institution, Woods Hole, Massachusetts

(Manuscript received 23 January 2005, in final form 18 August 2005)

ABSTRACT

The response of the North Atlantic thermohaline circulation to idealized climate forcing of 1% per year compound increase in CO_2 is examined in three configurations of the Community Climate System Model version 3 that differ in their component model resolutions. The strength of the Atlantic overturning circulation declines at a rate of 22%–26% of the corresponding control experiment maximum overturning per century in response to the increase in CO_2. The mean meridional overturning and its variability on decadal time scales in the control experiments, the rate of decrease in the transient forcing experiments, and the rate of recovery in periods of CO_2 stabilization all increase with increasing component model resolution. By examining the changes in ocean surface forcing with increasing CO_2 in the framework of the water-mass transformation function, we show that the decline in the overturning is driven by decreasing density of the subpolar North Atlantic due to increasing surface heat fluxes. While there is an intensification of the hydrologic cycle in response to increasing CO_2, the net effect of changes in surface freshwater fluxes on those density classes that are involved in deep-water formation is to increase their density; that is, changes in surface freshwater fluxes act to maintain a stronger overturning circulation. The differences in the control experiment overturning strength and the response to increasing CO_2 are well predicted by the corresponding differences in the water-mass transformation rate. Reduction of meridional heat transport and enhancement of meridional salt transport from mid- to high latitudes with increasing CO_2 also act to strengthen the overturning circulation. Analysis of the trends in an ideal age tracer provides a direct measure of changes in ocean ventilation time scale in response to increasing CO_2. In the subpolar North Atlantic south of the Greenland–Scotland ridge system, there is a significant increase in subsurface ages as open-ocean deep convection is diminished and ventilation switches to a predominance of overflow waters. In middle and low latitudes there is a decrease in age within and just below the thermocline in response to a decrease in the upwelling of old deep waters. However, when considering ventilation within isopycnal layers, age increases for layers in and below the thermocline due to the deepening of isopycnals in response to global warming.

1. Introduction

Interest in the behavior of the thermohaline circulation (THC) in global warming scenarios is motivated by several factors. The first is the close relationship between the THC and oceanic meridional heat transport, particularly at midlatitudes in the North Atlantic. A weakening of the THC and the accompanying decrease in meridional heat transport can result in significant regional differences in the response of surface temperature to increasing CO_2 relative to the zonal average at comparable latitudes (Wood et al. 2003). A second factor is the linkage of the THC to ocean ventilation, that is, the rate at which surface waters are subducted into the interior ocean. This process is, in turn, an important controlling mechanism in the rate of gas exchange be-

* The National Center for Atmospheric Research is sponsored by the National Science Foundation.

Corresponding author address: Dr. Frank O. Bryan, Climate and Global Dynamics Division, National Center for Atmospheric Research, P.O. Box 3000, Boulder, CO 80307.
E-mail: bryan@ucar.edu

tween the ocean and atmosphere and hence of central importance in the global carbon cycle (Sarmiento and Gruber 2002). Interest in the THC is heightened by studies suggesting that it has undergone abrupt changes in the past (Broecker 1997) and may do so in the future in response to certain climate change scenarios (Stocker and Schmittner 1997).

Previous studies with coupled climate system models have indicated a broad range of responses of the thermohaline circulation to global warming (see reviews by Cubasch et al. 2001; Wood et al. 2003): from no significant change (Latif et al. 2000; Bleck and Sun 2004) to near collapse at CO_2 levels equal to four times present conditions (Dixon et al. 1999). The Community Climate System Model version 3 (CCSM3) is the most recently released version of the National Center for Atmospheric Research (NCAR) Community Climate System Model (Collins et al. 2006a). Earlier versions of CCSM have shown relatively modest weakening of the North Atlantic meridional overturning circulation in response to increasing CO_2 (Gent 2001; Gent and Danabasoglu 2004; Hu et al. 2004). Our first objective in this study is to quantify the response of the THC to global warming in CCSM3 and to elucidate the processes involved in this response. In contrast to previous versions of CCSM (or most other coupled climate system models), coordinated experiments have been conducted at multiple resolutions, allowing us to determine the sensitivity of the simulated response to this choice of model configuration. Our second objective in this study is to quantify changes in ocean ventilation in response to global warming. This is facilitated by the inclusion of ideal age (Thiele and Sarmiento 1990) as a passive tracer in all of the experiments considered here. This passive tracer provides a direct (though only indirectly observationally verifiable) diagnostic of the model ventilation rate. We attempt to relate the response of ventilation to the changes in the THC through their common dependence on the processes of water mass transformation in the surface ocean. To maintain the focus on the connections with the THC, we restrict the analysis of ventilation processes to the Atlantic basin in the present study.

2. Model and experiment description

The CCSM3 is a fully coupled model of the physical climate system, comprised of the Community Atmosphere Model (CAM: Collins et al. 2006b), the Community Land Model (CLM: Dickinson et al. 2006), the Community Sea Ice Model (CSIM: Holland et al. 2006), and the Parallel Ocean Program (POP: Smith and Gent 2004). The system can be configured with component models at several resolutions. In this study we make use of three configurations. The first is a low-resolution version, referred to hereafter as T31x3, with an atmosphere model using spectral truncation of T31 (grid spacing of 3.75°) coupled to an ocean model on a grid with approximately 3° horizontal resolution. The sea ice component model runs at the same resolution as the ocean model, and the land surface model runs at the same resolution as the atmospheric model, though with a representation of subgrid-scale heterogeneity of surface types. The simulation of present-day climate of this version of CCSM3 is described in more detail in Yeager et al. (2006). The other two versions of the system, referred to hereafter as T42x1 and T85x1, both use the same ocean and sea ice models with a horizontal resolution of approximately 1°, the former coupled to an atmosphere using spectral truncation of T42 (grid resolution of 2.8°), the latter to an atmosphere using spectral truncation of T85 (grid resolution of 1.4°). Aspects of the climate of these higher-resolution versions of the system are described in more detail in Hack et al. (2006), Large and Danabasoglu (2006), Collins et al. (2006a), and references therein. At a number of points throughout this paper we indicate systematic changes in some property of the solution between model configurations as increasing or decreasing with resolution. The reader should note however that the increase in resolution between the T42x1 and T85x1 configurations is only in the atmospheric and land components and should understand that the change is systematic in the sequence: T31x3, T42x1, T85x1. Furthermore, each configuration has been tuned to a certain degree to provide a reasonable representation of present-day climate that is close to net energy balance in the control simulation. As a result, different choices of a number of parameters, such as the magnitude of subgrid-scale dissipation, may affect the results independent of the resolution itself.

The experiments used in this study comprise the initial suite of control runs with CCSM3 for present-day climate conditions and 1% per year increasing CO_2. For each of the three configurations described above, a control experiment for present-day climate conditions (CO_2 concentration equal to 355 ppm: the observed global mean value in 1990) is initialized with a resting ocean using the Poles Hydrographic Climatology, version 2 (PHC2; Steele et al. 2001). These experiments have been integrated for between 700 and 1000 years without flux correction. The transient climate forcing experiments (1% per year increasing CO_2) are branched from their respective control experiments at year 400, and CO_2 begins increasing at year 410. Doubling of CO_2 is thus reached at year 480, and quadrupling at year 550. Carbon dioxide stabilization experi-

TABLE 1. Component model resolution and climate statistics for each configuration.

Resolution		Sensitivity		Mean max	Mean vertical flux
Atmosphere	Ocean	Equilibrium (°C)	Transient (°C)	MOC (Sv)	60°–65° at 1000 m (Sv)
T31	~3°	2.3	1.37	15.3	5.0
T42	~1°	2.5	1.43	19.5	10.3
T85	~1°	2.7	1.46	21.8	10.6

ments are branched from the transient CO_2 cases at these dates with CO_2 held fixed at twice and four times present-day values respectively, and run for at least an additional 150 years. Additional transient CO_2 experiments have been conducted for the T42x1 and T85x1 configurations as part of a model porting validation test. Round-off level differences due to computer architecture and compiler differences lead to solution divergence, providing two ensemble members starting from the same initial condition. The results from those cases will be included here where appropriate.

The ideal age tracer evolves according to

$$\frac{\partial A}{\partial t} = L(A) + M(A) + 1, \tag{1}$$

where L and M are the same advection and mixing operators acting on potential temperature and salinity and the source term has strength of one unit per year. The age tracer is initialized to zero and has a surface concentration held fixed at zero. In the T42x1 control experiment, the ideal age tracer was not included in the first 275 years of the integration. Rather than initializing it with 0 at that date, the age distribution from the T85x1 control experiment at year 135 was used so that the ideal age distribution in the T42x1 experiment is not as fully spun-up as the others. The spinup of the deep age distribution occurs over very long time scales. For the purposes of this study we are focusing primarily on regions of deep-water formation and thermocline ventilation characterized by young ages and where the age distribution, even in the T42x1, has approached a statistically stationary value in the control experiments.

The equilibrium climate sensitivity (equilibrium global mean surface temperature response to instantaneous doubling of CO_2 of the atmospheric component model coupled to a mixed layer ocean) at each resolution is indicated in Table 1. The climate sensitivity has a range of 0.4°C across the three configurations, increasing with increasing resolution, and all three versions of CCSM3 have higher equilibrium climate sensitivity than the value of 2.2°C obtained with a T42x1 configuration of CCSM2, the previous generation version of this model (Kiehl and Gent 2004). The transient climate response (the global mean surface temperature response to 1% per year increasing CO_2 at the time of doubling) of the fully coupled system differs by less than 0.1°C across the three CCSM3 configurations (Table 1). The reduction in the spread of the transient response relative to the equilibrium response is consistent with results from a large number of coupled climate system models (Raper et al. 2002). Owing to an error in the treatment of the mixing ratio of CO_2 in transient forcing experiments in CCSM2, as described in Gent and Danabasoglu (2004), it is not possible to quantitatively compare the transient climate response of CCSM3 with earlier versions of the model. Other aspects of the climate sensitivity of CCSM3, based on results from these same experiments, are described in Kiehl et al. (2005) and Bitz et al. (2006).

3. Results

a. Response of the overturning circulation

While the focus of this study is the response of the North Atlantic circulation to transient climate forcing, we briefly describe the statistics of the equilibrium state of the control simulations as a basis for evaluating changes. More systematic evaluation of the simulated climate of the control experiments with respect to observations can be found in the references cited above. The time series of the maximum North Atlantic Eulerian-mean meridional overturning (MOC) streamfunction for the control experiments at each of the three resolutions is shown in Fig. 1 (the contribution of the eddy-induced overturning in midlatitudes of the North Atlantic is small). In each case, the overturning circulation experiences a rapid increase during the first 40 yr, followed by a slower decrease. The magnitude of this downward adjustment is larger and occurs over a longer time period at lower resolution, resulting in an asymptotic overturning strength that decreases with decreasing component model resolution. Two measures of the control experiment overturning strength are provided in Table 1. The first is the maximum of the overturning streamfunction in the North Atlantic below 500 m. The second, advocated by Gent (2001), is the sinking flux across the 1000-m depth level between 60° and 65°N. The trends in the maximum overturning in-

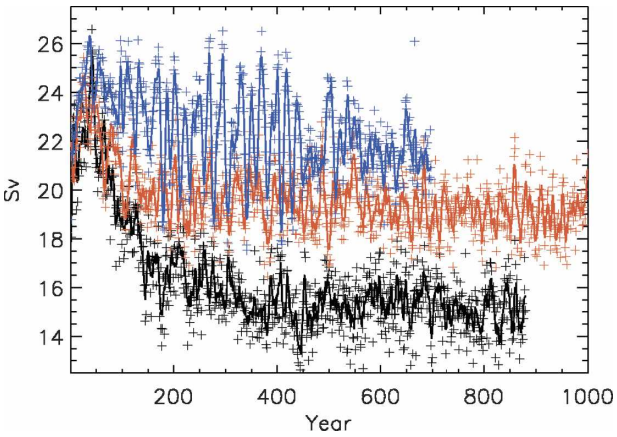

FIG. 1. Time series of maximum meridional overturning streamfunction in the North Atlantic (below 500 m) for present-day control experiments: T31x3 (black), T42x1 (red), and T85x1 (blue). Solid lines are time series smoothed with a 5-yr running mean filter; symbols are annual averages.

dex between years 350 and 850 for the control experiments are indicated in Table 2. A weak decrease in the overturning strength persists in all experiments, with larger (but still quite small) drift at higher resolution.

In addition to increasing mean overturning strength, the variability of the overturning in the control experiments increases with resolution, particularly between T42x1 and T85x1. The standard deviation of the 5-yr running mean smoothed and detrended time series of the maximum overturning between years 350 and 850 (350 and 700 for the T85x1 configuration) is also given in Table 2. There is a factor of 2 increase in the amplitude of the variability across this range of resolution. There appear to be qualitative changes in the character of the overturning variability in the T85x1 configuration around years 175 and 400. Between these years, a large amplitude oscillation with a period near 20 yr dominates the variability and is subsequently replaced by broader band and lower amplitude variability that more closely resembles the variability in the lower-resolution configurations.

The mean North Atlantic overturning streamfunctions averaged over years 401 to 600 of the control experiment at each resolution are shown in Figs. 2a–c. The T42x1 and T85x1 have qualitatively similar streamfunction distributions, with 10 to 11 Sv (Sv $\equiv 10^6$ $m^3\,s^{-1}$) of downwelling across 1000-m depth between 60° and 65°N (Table 1). The volume transport of southward-flowing water with $\sigma_\theta > 27.8$ across a grid line between Greenland and Iceland intersecting Denmark Strait is 2.3 Sv in T42x1 and 3.8 Sv in T85x1. Dickson and Brown (1994) estimate the transport of water with $\sigma_\theta > 27.8$ from moored current meter arrays upstream and downstream of this line as 2.9 Sv and 5.1 Sv, respectively. The simulation in the T85x1 configuration is thus within the range of the observations, while the T42x1 slightly underestimates the transport of dense water across the overflow. The difference in the maximum overturning between these two configurations arises primarily in the secondary region of downwelling between 45° and 50°N. This downwelling occurs broadly over the southern and eastern flanks of the subpolar gyre. Regions of downwelling velocities of comparable magnitude occur to the north and south of this latitude band but are partially balanced in the zonal integral by upwelling in the western basin. The northern branch of the sinking reaches its greatest depth in the T85x1 configuration. The T31x3 configuration stands apart from the other two configurations. The downwelling across 1000 m between 60° and 65°N is only half of that in the higher-resolution models (Table 1), and the overturning streamfunction does not show as clear an exchange between the Greenland–Iceland–Norwegian (GIN) Seas and the subpolar North Atlantic: there is no southward flowing water in Denmark Strait with $\sigma_\theta > 27.75$, and only 1.9 Sv considering waters denser than $\sigma_\theta > 27.5$. The depth of the southward flowing branch of the overturning cell is shallowest in the T31x3 configuration. Note that, in addition to the lower horizontal resolution of the component models, the 3° ocean component has coarser vertical resolution

TABLE 2. Trend in maximum North Atlantic overturning computed from time series shown in Fig. 3 with a 5-yr running mean filter. Standard deviation of the detrended and smoothed time series.

		T31x3		T42x1		T85x1	
Expt	Years	Trend (Sv century^{-1})	Residual std dev (Sv)	Trend (Sv century^{-1})	Residual std dev (Sv)	Trend (Sv century^{-1})	Residual std dev (Sv)
Control	350–850	−0.03	0.63	−0.11	0.72	−0.28*	1.24*
1% expt a	410–560	−3.28	0.57	−4.84	0.55	−5.18	0.87
1% expt b				−4.46	0.60	−5.57	1.08
2x capped	530–630	0.05	0.65	0.43	0.55	0.51	0.51
4x capped	600–700	−0.21	0.53	1.13	0.50	1.05	0.40

* Computed over years 350–700.

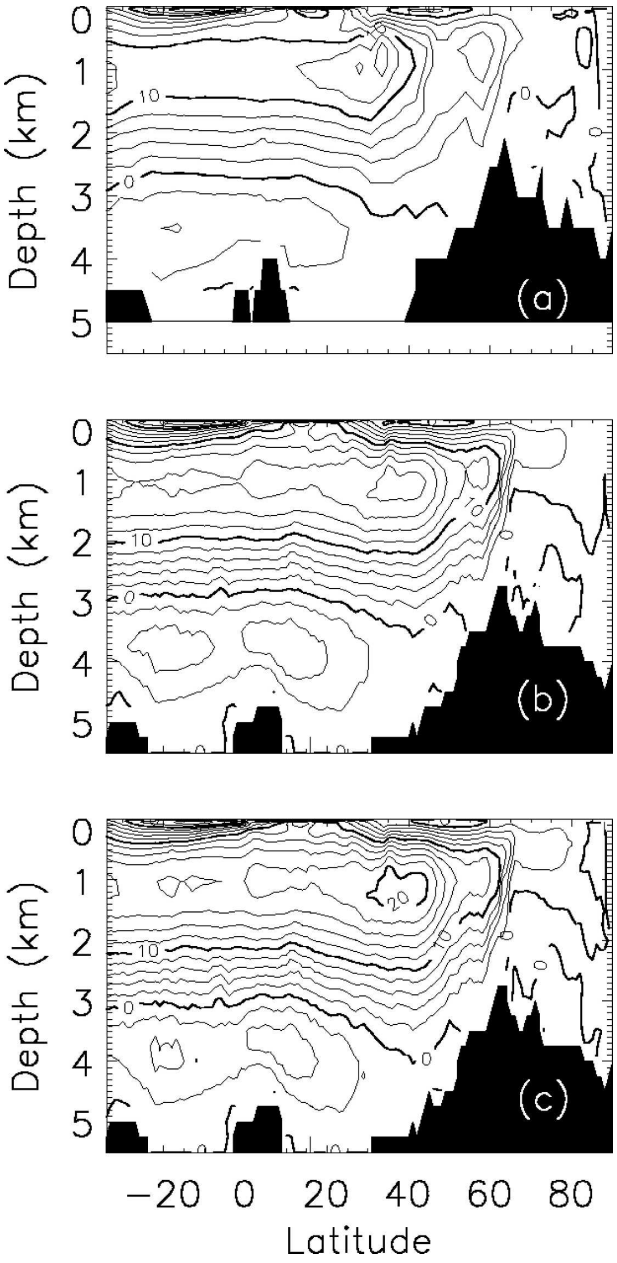

FIG. 2. Streamfunction for Atlantic Eulerian-mean meridional overturning circulation in control experiments averaged over years 401–600; contour interval is 2 Sv. (a) T31x3, (b) T42x1, and (c) T85x1.

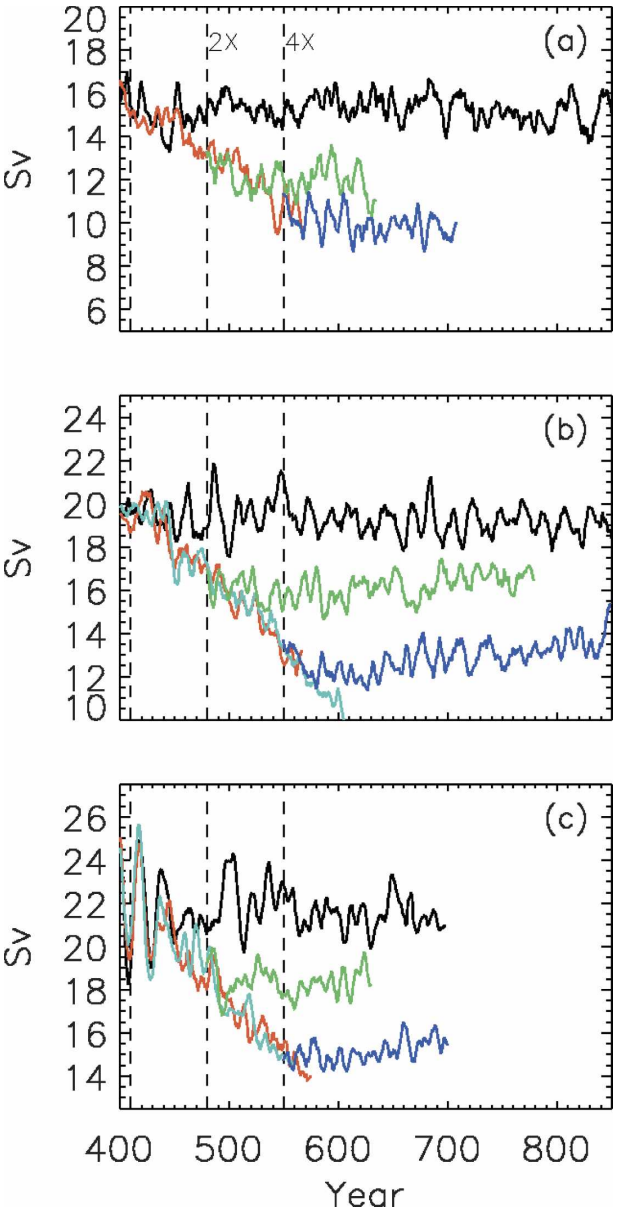

FIG. 3. Response of North Atlantic maximum overturning streamfunction to transient climate forcing for (a) T31x3, (b) T42x1, and (c) T85x1. Control experiment is shown in black, transient experiments in red and cyan, double CO_2 stabilization in green, and quadruple CO_2 stabilization in blue. Note that the ordinate is shifted, but the range is the same in each.

and a maximum depth of 5000 m rather than 5500 m as in the 1° ocean component, with consequent differences in the topography and sill depths.

The response of the North Atlantic maximum MOC to increasing CO_2 for each resolution is shown in Figs. 3a–c. Note that for the T42x1 and T85x1 cases two transient CO_2 experiments are shown. For each configuration, the MOC starts to decline from the mean value of the control experiment after about 40 yr of increasing CO_2, resulting in a relatively modest weakening of 2 to 2.5 Sv at the time of CO_2 doubling. The trends in the maximum overturning circulation index over years 410 to 560 (up to the time of CO_2 quadrupling) for each resolution are indicated in Table 2. The response of the MOC to increasing CO_2 exceeds the drift in the control experiments by more than one order

of magnitude in all cases. In absolute terms, the magnitude of the rate of decline of the MOC increases with increasing resolution from a low of 3.3 Sv century^{-1} to a high of 5.6 Sv century^{-1}. In relative terms however, the decline is more uniform, varying between 22% and 26% of the control experiment maximum overturning strength per century.

As noted above, there is larger variability in the overturning, particularly at decadal time scales in the T85x1 control experiment than in the experiments with lower-resolution models. There is an indication, though not a strongly significant one, of a suppression of this variability during the period of transient climate forcing. The standard deviation of the detrended time series of maximum overturning (after smoothing with a 5-yr running mean filter) is shown in Table 2 for each experiment. The T31x3 configuration shows a decrease of decadal variability of 10% relative to the corresponding control experiment, while the T85x1 experiments show a decrease of 20%–30%. This suppression of variability persists into the period of stabilized CO_2.

Following stabilization of CO_2 in the T42x1 and T85x1 configurations, the strength of the MOC continues to decline for a few decades, but then begins to recover. The rate of recovery is higher for the experiments with CO_2 stabilized at quadruple present-day concentrations than for the experiments stabilized at double present-day concentrations (Table 2). This is somewhat at odds with the results of Manabe and Stouffer (1994) where the MOC recovers completely over a period of several centuries for a double CO_2 experiment, but remains in a collapsed state for a quadruple CO_2 experiment. Again, the T31x3 configuration stands apart from the others: the overturning continues to decline through the length of the experiment following stabilization at quadruple present-day CO_2, and the recovery is very weak for stabilization at double present-day CO_2.

The MOC streamfunction at the time of CO_2 quadrupling at each resolution is shown in Fig. 4. Both the sinking near the overflows and the secondary sinking between 45° and 50°N decline at all resolutions. The maximum depth of the northern branch of the sinking decreases by 500–700 m, more so in the higher-resolution experiments, so that the depth of the overturning cell is more comparable across configurations in the transient forcing experiments than in the control experiments.

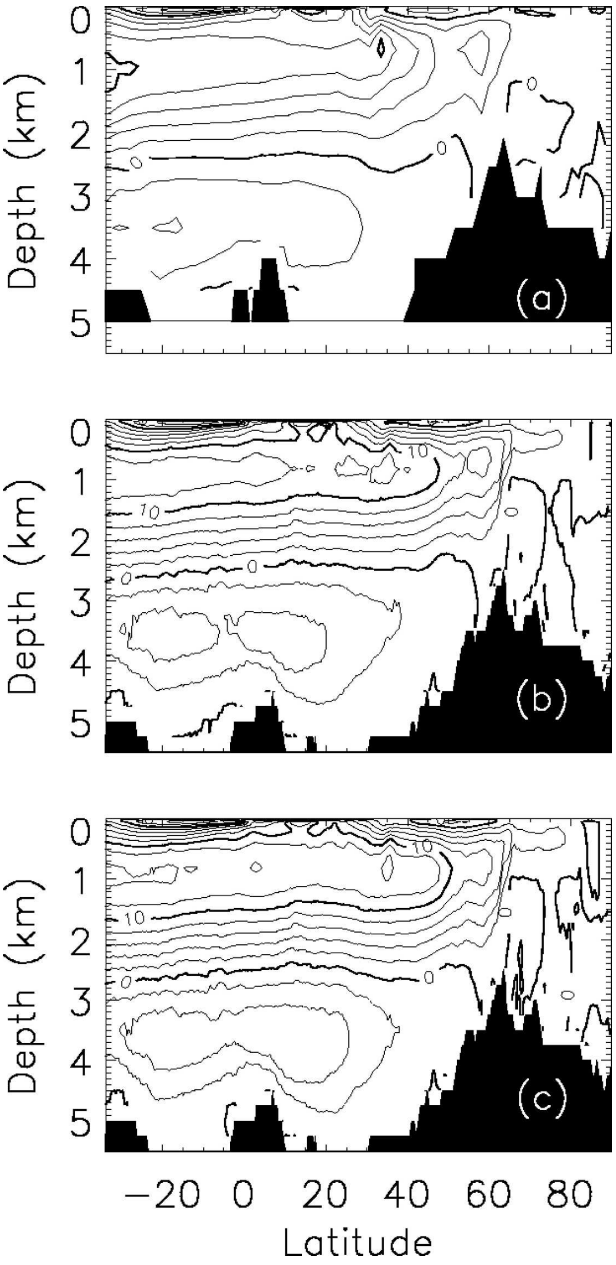

FIG. 4. Streamfunction for Atlantic meridional overturning circulation in transient CO_2 experiments for years 541–560 (20-yr period centered on time of quadrupling of CO_2); contour interval is 2 Sv. (a) T31x3, (b) T42x1 (average of two ensemble members), and (c) T85x1 (average of two ensemble members).

b. *Processes controlling the response of the overturning circulation*

The annual mean surface density and the maximum mixed layer depth over the North Atlantic region for the T85x1 control experiment is shown in Fig. 5a. The sites of deep-water formation, as indicated by the deepest mixed layers, are found in three locations: in the GIN Seas in a band along the ice edge (the position of the ice edge is indicated in Fig. 6) extending northeastward from Iceland to Spitzbergen, along the southern flank of the Greenland–Iceland–Scotland ridge system,

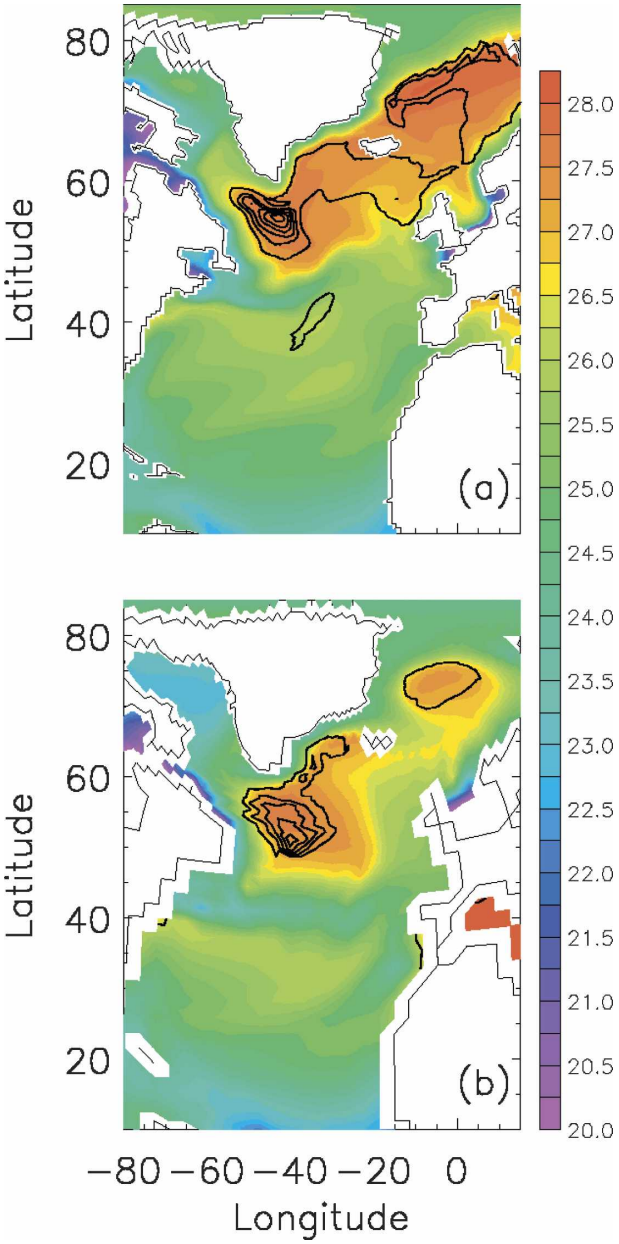

FIG. 5. Surface density (color) and annual maximum mixed layer depth (contours at intervals of 400 m, beginning at 400 m) averaged over years 541–560: (a) T85x1 control experiment and (b) T31x3 control experiment.

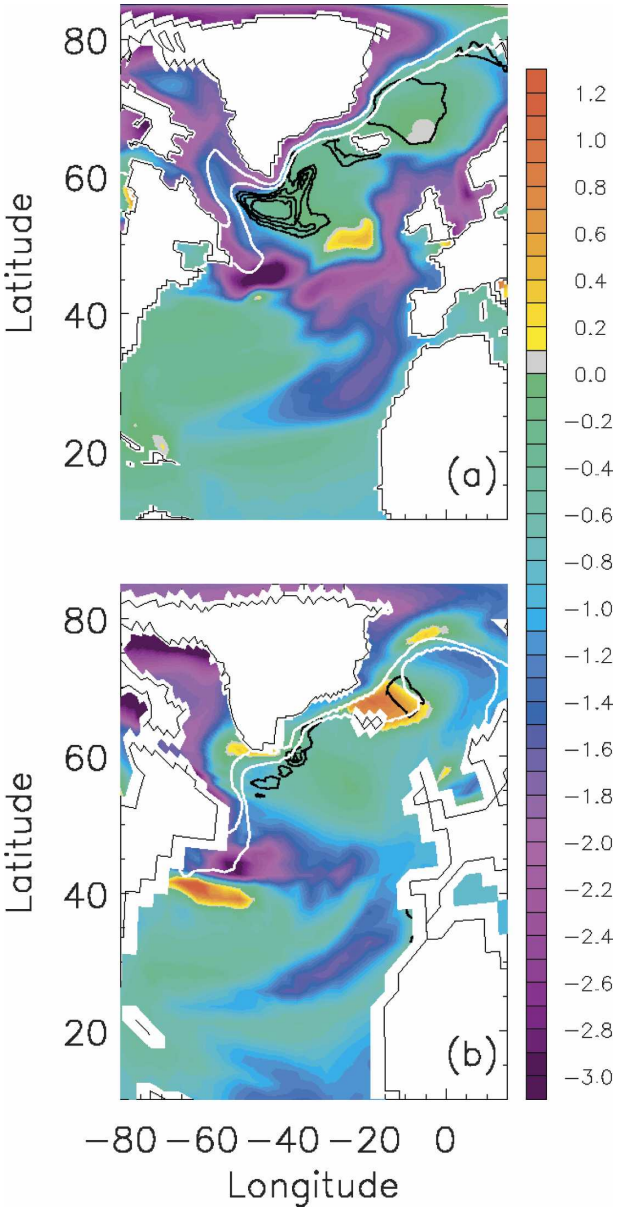

FIG. 6. Change in surface density between control experiment and transient forcing experiment at the time of CO_2 quadrupling (color), annual maximum mixed layer depth (contours at interval of 400 m, beginning at 400 m), and winter (January–March) mean sea ice extent in the control and transient experiments (white contours) averaged over years 541–560: (a) T85x1 configuration and (b) T31x3.

and in the central subpolar gyre south of Cape Farewell spanning the Labrador and Irminger Basins. Maximum mixed layer depths reach 800–1000 m in the GIN Seas, and over 2000 m south of Cape Farewell. The T42x1 configurations have qualitatively similar distributions, though the area of deep mixed layers between 50° and 60° is displaced several degrees of longitude to the east and does not extend as far into the Labrador Sea. The T31x3 configuration differs more fundamentally (Fig. 5b): it lacks a zone of deep mixed layers extending along the Greenland–Iceland–Scotland ridge system, has lower density in the regions of maximum mixed layer depths, and the area of deep mixed layers to the south of Greenland is displaced farther to the south and east. The more extensive ice coverage in this configuration (Yeager et al. 2006) restricts the area of deep mixed layers to a more central area of the GIN Seas.

The change in surface density between the T85x1 transient experiment and control and the maximum mixed layer depths at the time of CO_2 quadrupling are shown in Fig. 6a (note that the contours represent the *values* at the time of doubling, and the colors a *change* at the time of doubling). The decrease in surface density is largest around the periphery of the subpolar gyre, especially in the East Greenland Current and Labrador Current. The density change is smallest in the central gyre, and even increases slightly in some areas. Thus, surface density changes are minimized in the regions of deep-water formation. The maximum mixed layer depths decrease in each of the three deep-water formation regions noted above, but still reach 1600 m south of Cape Farewell and over 500 m in the GIN Seas. In the T31x3 configuration (Fig. 6b), the decrease in mixed layer depths is larger and more spatially extensive. The change in surface density shows several notable differences from the higher-resolution configurations. There is an increase in density along the Gulf Stream, in the area north of Iceland where the winter sea ice extent has retreated, and in smaller areas in the Labrador and northern GIN Seas near the ice edge. The decrease in density is smaller in the East Greenland Current region and along the southern and eastern boundaries of the subpolar gyre than in the higher-resolution configurations

The contributions of temperature changes, $\delta\theta$, and salinity changes, δS, to the change in surface density, $\delta\rho$,

$$\delta\rho = \rho_0(\alpha\delta\theta + \beta\delta S), \tag{2}$$

between the control and transient experiments at the time of CO_2 quadrupling for the T85x1 and T31x3 configurations are shown in Fig. 7. For the T85x1 configuration, the temperature contribution is negative (decreasing density) everywhere over the North Atlantic basin except in a small region in the North Atlantic Current. The salinity contribution is positive, compensating for much of the density decrease due to increasing temperature, over the central subpolar gyre, as well as the western subtropical gyre. The salinity compensation is especially strong in the deep-water formation region in the western GIN Seas and north of Iceland. In contrast, the salinity contribution is negative, enhancing the decrease in density due to warming, around the periphery of the subpolar gyre. In the T31x3 configuration (Figs. 7c and 7d), the area of positive contribution of salinity to density changes is less spatially extensive in the subpolar gyre, but locally stronger in magnitude north of Iceland where the ice edge has retreated. There is weaker compensation between the temperature and salinity contributions to density change in the region of deep mixed layers between 50°

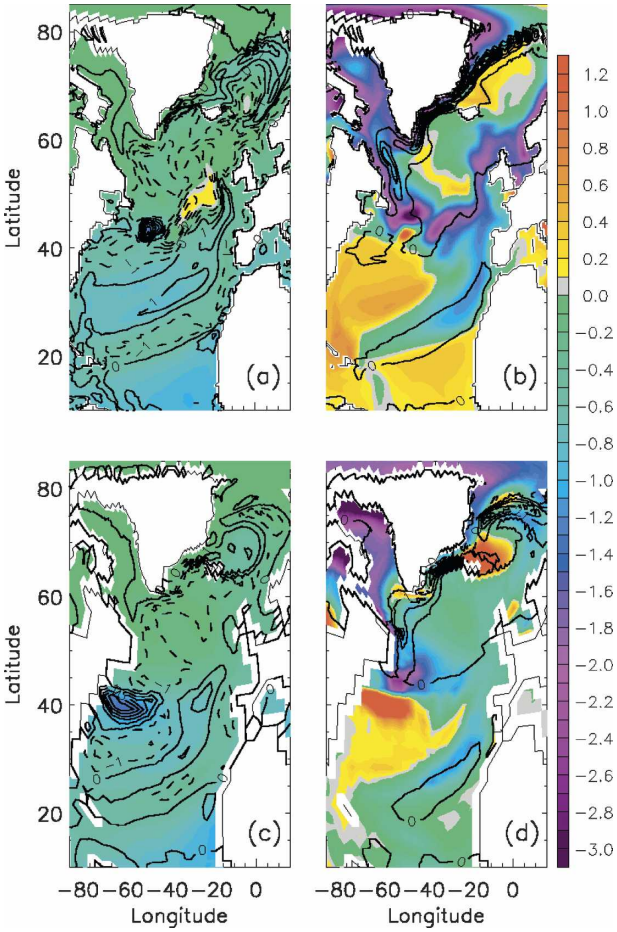

FIG. 7. Contribution to change in surface density between T85x1 control and transient experiment at time of CO_2 quadrupling from (a) temperature (color) and change in contribution to surface density flux from heat flux [contours at intervals of 1 mg m^{-2} s^{-1}; negative values (decreasing density) are dashed] and from (b) salinity (color) and change in contribution of surface density flux from freshwater fluxes (contours at intervals of 1 mg m^{-2} s^{-1}) for T85x1 configuration. (c) As in (a) except for T31x3 configuration; (d) as in (b) except for T31x3.

and 60°N resulting in larger decreases in density than in the higher-resolution configurations, and consequently more extensive retreat of the region of deep mixed layers.

The changes in the contributions of the heat flux, F_{heat}, and freshwater flux, F_{water}, to the change in total surface density flux F_ρ,

$$F_\rho = \frac{\alpha}{\rho_0 c_p} F_{\text{heat}} - \beta F_{\text{water}}\left(\frac{S}{1-S}\right), \tag{3}$$

between the transient experiments and the control experiments for the T85x1 and T31x3 configurations are shown as contours in Fig. 7. Note that the heat and freshwater fluxes in Eq. (3) include contributions from

ocean–ice exchange and continental runoff as well as ocean–atmosphere fluxes. Considering the T85x1 configuration first, over most of the subpolar basin, the heat flux into the ocean increases, making the density flux more negative, that is, decreasing densification. Note that the heat flux contribution to the density flux change is strongly anticorrelated with the temperature contribution to the density changes in a few regions such as along the path of the North Atlantic Current near 45°N, 45°W and around the northern perimeter of the GIN Seas. These regions experience a warming due to shifts in the current or as the ice area shrinks, but enhanced heat flux out of the ocean. The only area where there is an obvious local relationship between the salinity contribution to surface density changes and the freshwater flux contribution to the density flux changes is the dipole structure near the ice edge east of Greenland. Here, the marginal ice zone retreats toward the coast (Fig. 6), resulting in reduced freshwater input from ice melt, less negative surface density fluxes and increased density due to increasing salinity offshore, and the opposite near the new ice edge position. Over much of the basin, the surface density changes due to salinity are not closely related to the local freshwater contribution to the density flux, and hence must arise from changes in advective transport. We address this further below. The changes in surface density and surface buoyancy fluxes in the T42x1 configuration are quite similar to those described above for the T85x1 configuration, with modest differences in magnitude. The T31x3 configuration exhibits more substantial differences. The magnitude of the change in the heat flux contribution is smaller over the interior subpolar gyre. The sign of the change in the heat flux contribution to the density flux is positive, that is, greater densification in the area north of Iceland where the sea ice retreats during warming. There is a larger region of strong densification along the Gulf Stream.

The changes in the density and buoyancy forcing described above have a complex distribution that is difficult to interpret directly in terms of impact on deep-water formation processes. The water-mass transformation function (Speer and Tziperman 1992; Doney et al. 1998) provides a compact representation of the effect of the surface buoyancy fluxes on the surface density field. It is given by the integral of the surface density flux over the area of density outcrops,

$$T(\rho)\Delta\rho = \frac{1}{\tau}\int_{\tau}\iint_{\text{outcrop}} F_{\rho}\delta(\rho, \rho + \Delta\rho)\, dA\, dt, \qquad (4)$$

where $\delta(\rho, \rho + \Delta\rho)$ takes the value 1 for densities in the range ρ to $\rho + \Delta\rho$ and 0 elsewhere. The divergence of the transformation in density space, $-\partial T/\partial\rho$, provides a measure of the water-mass formation rate. The water-mass transformation rates for the control and transient experiments averaged over the 20-yr period bracketing the time of CO_2 quadrupling are shown in Fig. 8. Equation (4) is evaluated using a density interval of 0.1 kg m^{-3} and using monthly mean surface heat and freshwater fluxes, temperature, and salinity. The T42x1 and T85x1 control experiments show two density ranges with positive water mass formation, one centered on $\sigma_\theta = 26.5$, that is, subtropical mode water, and one between $\sigma_\theta = 27.5$ and 28.25, that is, subpolar mode water and deep water. The T31x3 configuration shows net formation in the same subtropical mode water range, but no subpolar mode water formation at densities higher than $\sigma_\theta = 28.0$. Furthermore, there is less distinct separation between the two classes of water mass formation in this configuration. The magnitude of

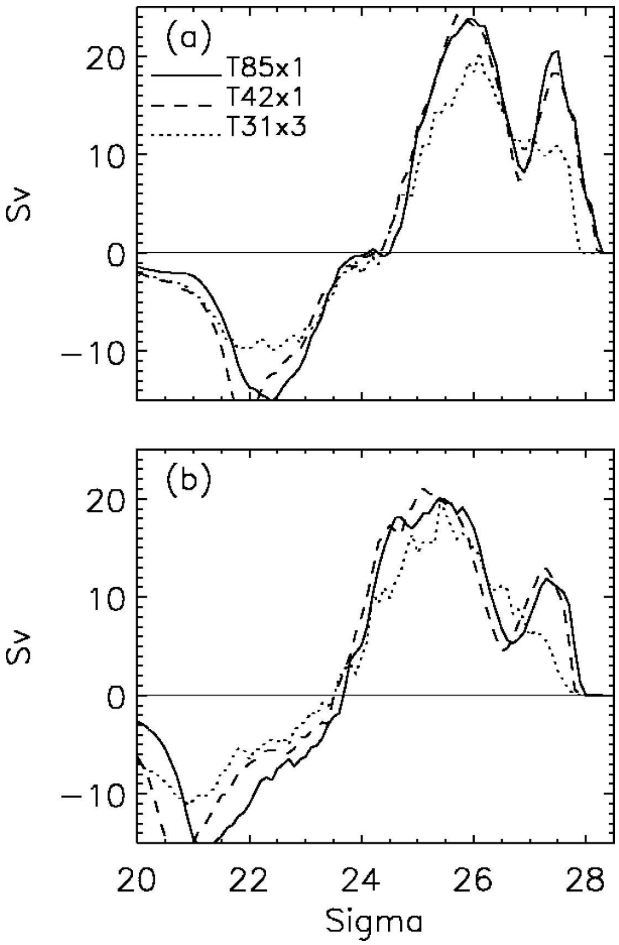

FIG. 8. Water-mass transformation rate for the North Atlantic basin averaged over years 541–560. (a) Control experiments and (b) transient forcing experiments: T85x1 (solid), T42x1 (dashed), and T31x3 (dotted).

the local maximum in the transformation rate at σ_θ = 27.5 corresponds quite closely to the strength of the control experiment maximum overturning in the T42x1 and T85x1 cases but underestimates it in the case of the T31x3.

At the time of CO_2 quadrupling the changes in the transformation rate show two main patterns. First, there is an overall shift of the function to lower density with the shape largely preserved, but with somewhat stronger effect in the lighter density classes (cf. the displacement of the overall minimum near σ_θ = 22 to that of the local minimum near σ_θ = 26.75). The geographical distribution of surface density fluxes does not shift appreciably as the climate warms, but the surface density decreases over most of the subtropics, resulting in the shift of the transformation curve in density space. The second notable feature is a decline in the rate of subpolar mode water formation. In the case of the T42x1 and T85x1 configurations, the decline of 5 to 8 Sv corresponds quite closely to the decline in the maximum overturning rate. In the case of the T31x3 configuration, the decline occurs in such a way that there is no longer a clear distinction in the subtropical and subpolar water mass formation densities, with weak formation rate across the whole range of densities higher than σ_θ = 25.5. For all configurations the decline in the rate of subtropical mode water formation is less pronounced than that of subpolar mode water formation, amounting to a decrease of 2–3 Sv.

The changes in the transformation rate evaluated separately for the GIN Seas and for the subpolar North Atlantic (including the Labrador Sea) are shown in Fig. 9 for each configuration. First, we note that, for the control experiments, the water mass formation in the GIN Seas occurs at higher density than in the subpolar North Atlantic in the T85x1 and T42x1 configurations, whereas the reverse is true in the T31x3. This accounts for the small flux of dense water through Denmark Strait in the low-resolution model, as noted above. Second, in each configuration, the change in the transformation rate in the GIN Seas region is characterized by a shift to lower density, with little change in the magnitude of the maximum: for example, the transformation rate at σ_θ = 27.5 for the T85x1 and T42x1 configurations does not decrease substantially between the control and the transient forcing case. This implies net water-mass formation at approximately the same rate, but in a lighter density class. In contrast, the transformation rate in the subpolar North Atlantic decreases in magnitude across the whole range of densities, implying a decrease in the net formation rate of dense water masses south of the overflows.

The contributions of the heat flux and freshwater flux

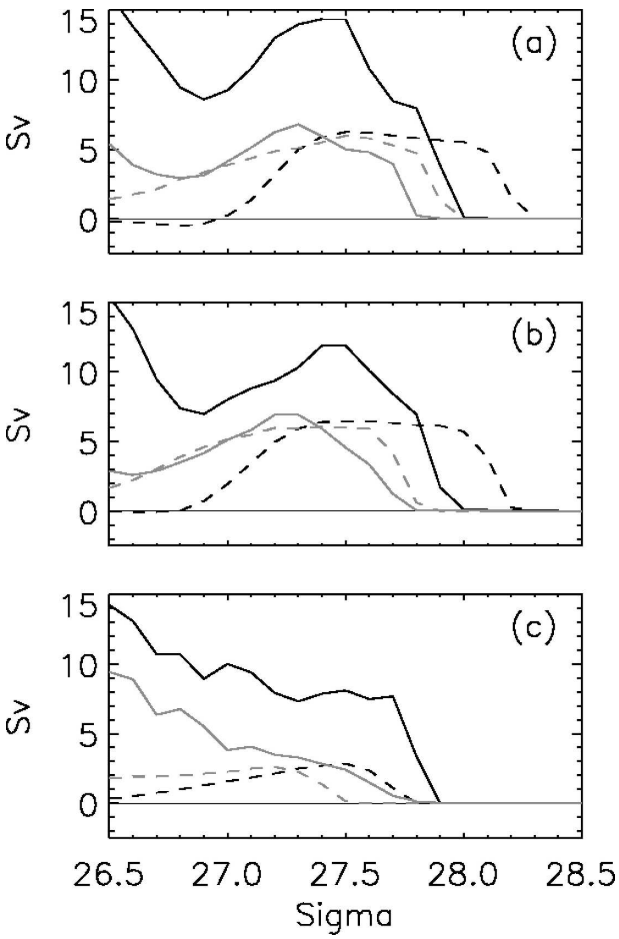

FIG. 9. Water mass transformation for the subpolar North Atlantic (solid) and the Greenland–Iceland–Norwegian Seas region (dashed), averaged over years 541–560 of the control (black) and transient forcing (gray) experiments: (a) T85x1, (b) T42x1, and (c) T31x3.

to the transformation rate for the control and transient experiments at the time of CO_2 quadrupling are shown in Fig. 10. The reduction in subpolar mode water formation is due to a decrease in the densification by heat fluxes. For all three configurations, the magnitude of the negative transformation due to freshwater fluxes, that is, the decrease of density due to freshening, is reduced in the subpolar mode-water density range. This is, in part, due to a reduction in the amount of melting ice reaching the deep-water formation zone in the GIN Seas as the ice retreats northward and westward. The net change in subpolar mode water formation is thus less than would be the case were heat fluxes alone acting on the ocean density. This is despite the fact that there is an intensification of the hydrologic cycle: the basin-mean freshwater flux into the ocean increases in the subpolar North Atlantic, but this addition of fresh-

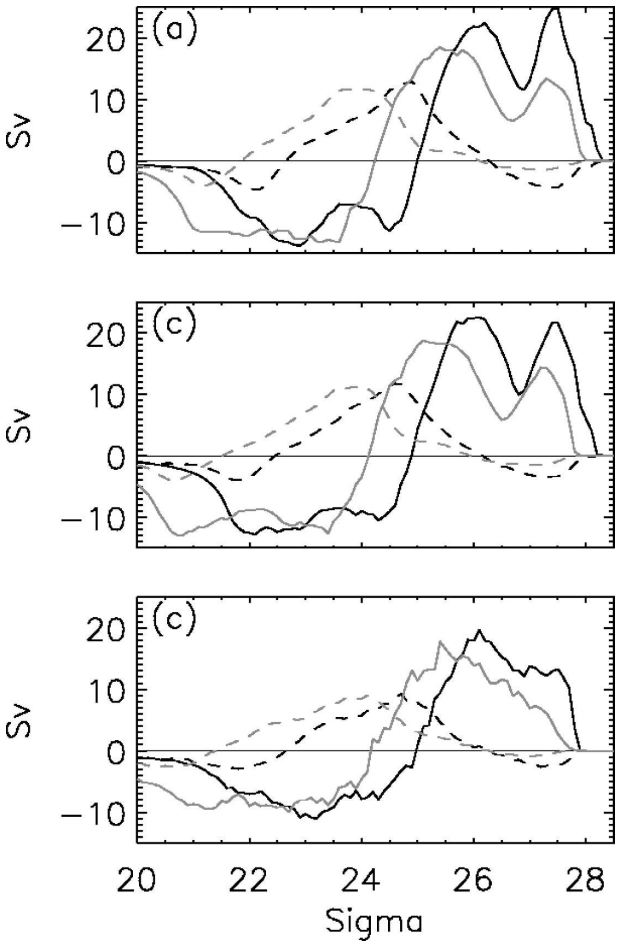

FIG. 10. As in Fig. 9 but for contributions of heat (solid) and freshwater fluxes (dashed) to the water-mass transformation rate.

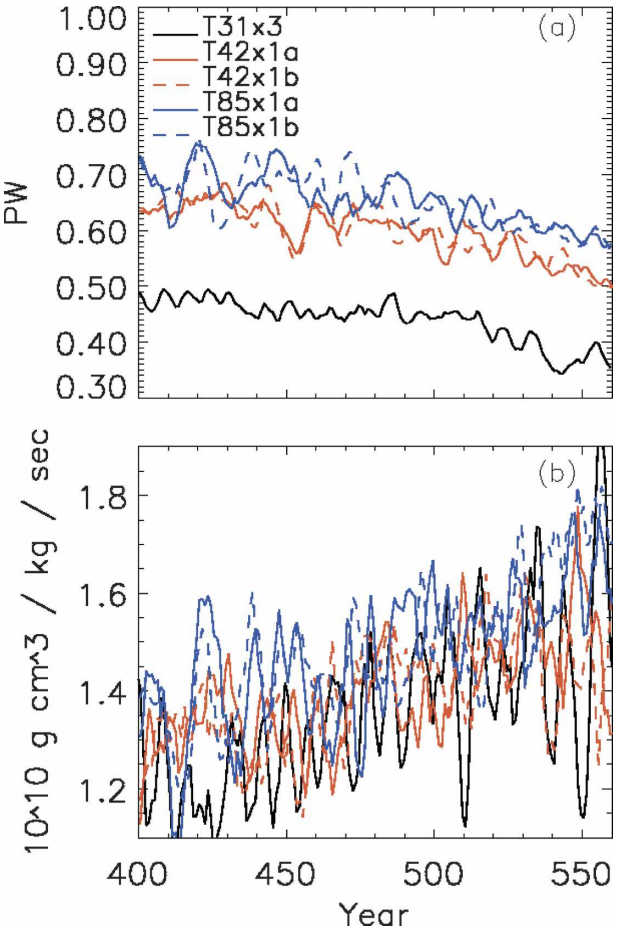

FIG. 11. (a) Time series of northward (a) heat transport and (b) salt transport across 55°N in the Atlantic for all transient forcing experiments.

water occurs primarily over a lighter density class around the perimeter of the basin.

As noted above, changes in surface salinity are not closely related to local changes in surface freshwater flux. Transport is a dominant contribution to changes in salinity over most of the basin during warming. As an integral measure of this we show the time series of the northward heat and salt transport across 55°N for each of the transient experiments in Fig. 11. The decrease in meridional heat transport and increase in meridional salt transport are both stabilizing influences on the thermohaline circulation by acting to maintain higher densities in the subpolar region. This result is consistent with those of Latif et al. (2000) and Thorpe et al. (2001). Bitz et al. (2006) show that heat transport poleward of 60°N increases (though by a smaller amount than in the subtropical decrease) with increasing CO_2. Thus, the changes in transport act to decrease the convergence of heat in the subpolar North Atlantic, counteracting a portion of the increased surface heating.

c. *Ventilation*

We first consider ventilation processes in the GIN Seas region, which has been identified as a key region for maintaining the strength of the overturning circulation (Schweckendiek and Willebrand 2005). Ideal age provides a measure of the time since a water parcel was last in the surface mixed layer, in contact with the atmosphere. In Fig. 12 we show, for each experiment, the volume of water in the GIN Seas region with decadal mean age less than 1 yr: an indication of the volume of water actively involved in convection each year. First, we note that, in the control experiments, the volume of new water increases with increasing resolution, as did the overturning strength and the water mass transformation into the subpolar mode-water density range. The disparity between the T31x3 and the other two configurations is a factor of 3.5 to 4, again reflecting the low water-mass formation rate in that configuration. In the T42x1 and T85x1 transient CO_2 experiments the

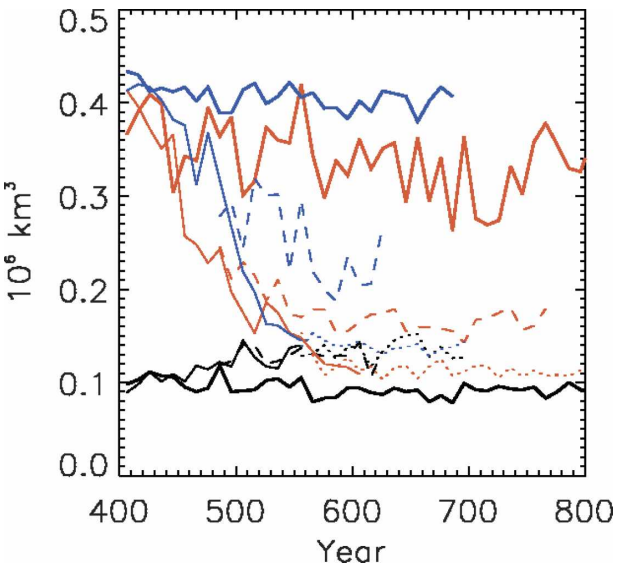

FIG. 12. Volume of water in the GIN Seas region with decadal mean age less than 1 yr. Control experiments are shown as thick solid, transient experiments as thin solid, 2x stabilized CO_2 experiments as dashed, and 4x stabilized CO_2 experiments as dotted lines. T31x3 experiments are black, T42x1 experiments are red, and T85x1 experiments are blue.

volume of new water begins decreasing shortly after the onset of CO_2 increase, in contrast to the decline of the overturning which is delayed by several decades. The T31x3 case behaves in an entirely different manner, with the volume of new water actually increasing as CO_2 increases. This appears to be related to enhanced convection in the region of ice retreat north of Iceland. There appears to be little or no recovery in the production of new water during the CO_2 stabilization experiments, in contrast to the overturning rate itself.

South of the overflows, in the subpolar North Atlantic, there are significant changes in the ventilation process associated with changes in the THC. The distribution of age and the velocity field at 1880 m (in the depth range of the southward branch of the overturning streamfunction) for the T31x3 and T85x1 experiments are shown in Fig. 13. For both configurations, minimum ages in the control experiment at this depth are located south of Cape Farewell where the winter mixed layer depths are maximum. In the T85x1 configuration, water with low ages is also seen to enter from the north through Denmark Strait. At both resolutions, at the time of CO_2 quadrupling, the low ages in the central subpolar gyre disappear. In the T85x1 configuration, this depth level is still ventilated from the north through Denmark Strait, whereas in the T31x3 configuration no ages less than 60 yr are found.

When considering the response of ventilation processes to global warming from the perspective of how they might influence CO_2 uptake, we need to consider the thermocline at all latitudes, not just the deep-water formation regions. The zonal average age in the upper 1000 m of the Atlantic for the T85x1 control and tran-

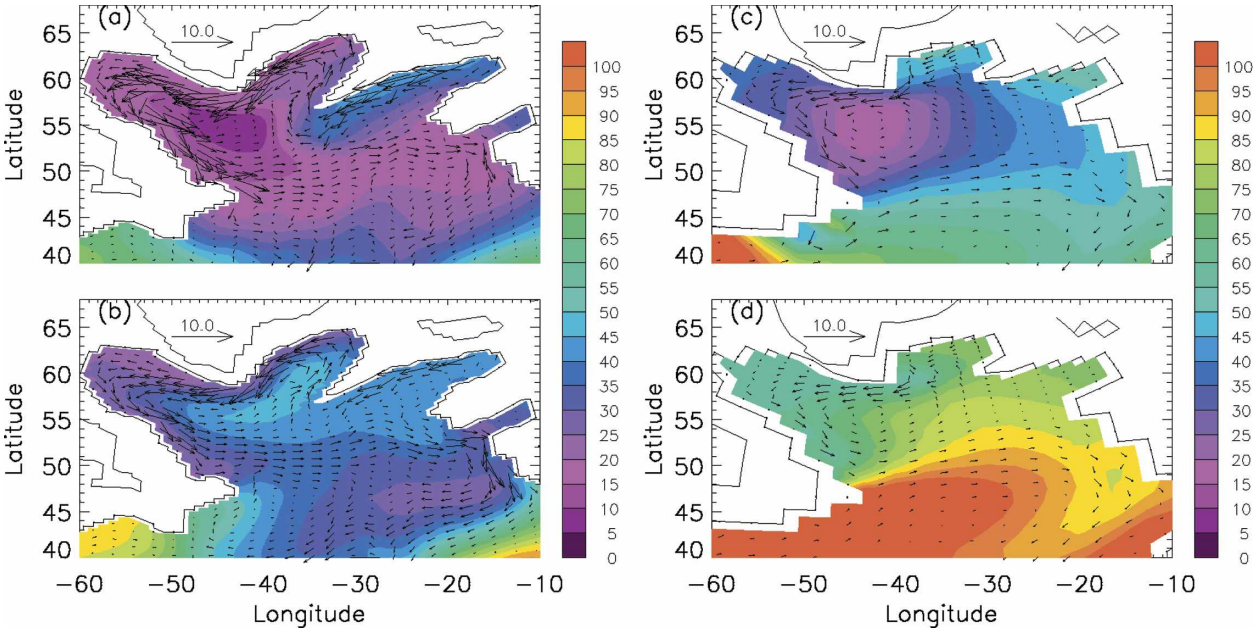

FIG. 13. Ideal age and velocity distribution at 1880 m for (a) T85x1 control experiment, (b) T85x1 transient experiment at time of quadrupling CO_2, (c) T31x3 control experiment, and (d) T31x3 transient experiment at time of quadrupling.

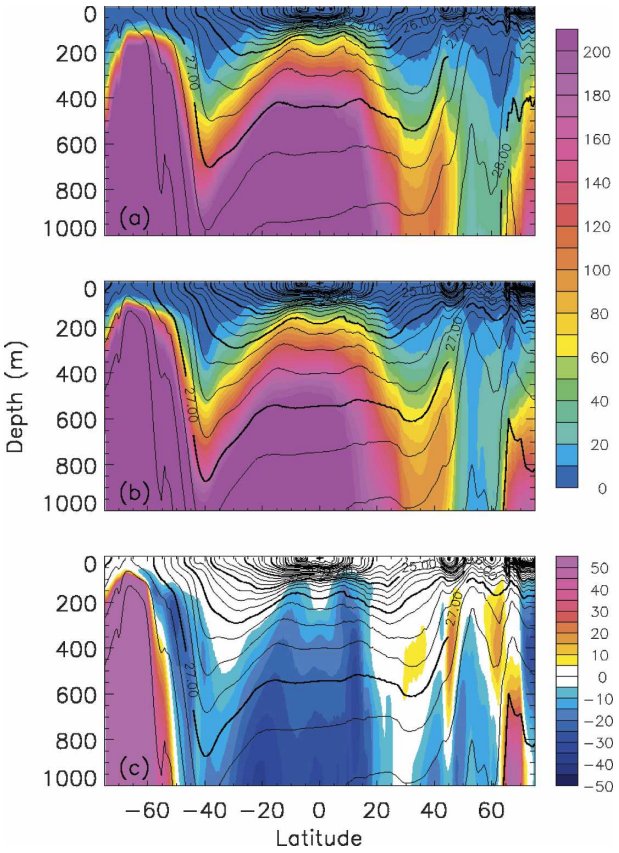

FIG. 14. (a) Zonally averaged ideal age (color) and potential density (contours at interval of 0.25) for (a) the T85x1 control experiment and (b) the T85x1 transient forcing experiment for years 540–561. (c) Change in age between the control and transient forcing experiments.

sient experiments, and their difference at the time of CO_2 quadrupling, is shown in Fig. 14. Averaged in level coordinates, the dominant signal in the difference field over most of the mid- and low-latitude upper Atlantic Ocean is a decrease in age, with the largest changes just below the thermocline in the Tropics. This is a consequence of reduced upwelling of old water as the thermohaline circulation strength declines. For all three configurations, the net vertical flux across 1000 m between 20°S and 20°N changes from weakly (0.5 to 0.9 Sv) upward to weakly (−1.9 to −2.3 Sv) downward. The large decrease in age below 500 to 1000 m is probably not a significant factor for CO_2 uptake because the initial ages are so old (>100 yr). The relatively small changes in age in the upper thermocline in the subtropics are consistent with the relatively small changes in the water-mass transformation rate for densities below $\sigma_\theta = 26.5$.

The second dominant signal in the change in zonal mean age (Fig. 14) is the large subsurface increase in age poleward of 60° latitude in each hemisphere. This increase is associated with the reduction of deep-water formation discussed above for the North Atlantic and a corresponding zone of the South Atlantic. Below approximately 2000 m, the age increases at all latitudes. Bitz et al. (2006) provide further discussion of age changes in the Southern Ocean and Arctic in these experiments.

The zonal average potential density is also shown in Fig. 14. As the thermohaline circulation weakens and the interior ocean warms, isopycnal surfaces deepen. The descent of isopycnals is, on average, greater than the descent of isosurfaces of age, such that the mean age on isopycnals near and below the base of the thermocline increases. The change in isopycnally averaged ideal age for the Atlantic for each configuration is shown in Fig. 15. For densities in the range of $\sigma_\theta = 25$ to 27, isopycnally averaged age increases with increas-

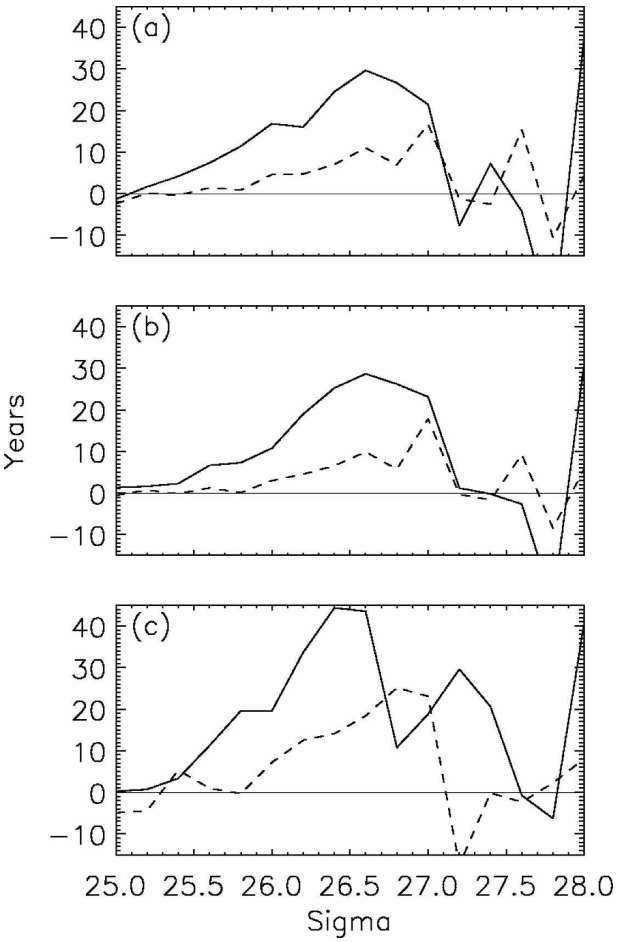

FIG. 15. Change in isopycnally averaged ideal age for the Atlantic basin (excluding the Labrador and GIN Seas) for the time of CO_2 doubling—years 471–490 (dashed)—and quadrupling—years 541–560 (solid): (a) T85x1, (b) T42x1, and (c.) T31x3.

ing CO_2, with the T31x3 configuration showing the largest magnitude change. The maximum increase of 30–45 yr at the time of CO_2 quadrupling occurs near σ_θ = 26.5, which is in the region of rapid increase of age with depth in the thermocline. This change represents an increase of approximately 75% of the isopycnal mean age of the control experiments on that density horizon. The reduced ventilation of these isopycnal layers would suggest reduced CO_2 uptake under global warming, consistent with a number of previous studies, for example, Sarmiento et al. (1998).

4. Discussion

As discussed in the introduction, there is a wide spread in the response of the thermohaline circulation to increasing CO_2 among different coupled climate system models. Here we have examined the differences in the response between three configurations of the CCSM3 that differ in their component model resolutions but utilize the same physical parameterizations and that have been tuned, to a certain degree, to produce the same gross climate statistics for present-day conditions. Despite this level of commonality, we find substantial differences in both the mean state of the THC and its response to global warming between the three configurations. This is especially true between the T31x3 and the two higher resolution configurations. This raises the question as to whether the difference in the atmosphere or ocean component resolution is responsible. Unfortunately we cannot definitively answer this question with the current set of experiments as we lack a case were the ocean resolution is changed while the atmospheric model resolution is held fixed, for example, a T31x1 or a T42x3 configuration. The results of Schweckendiek and Willebrand (2005) suggest that the representation of processes in the GIN Seas region in the ocean model, or the atmospheric model, is the most likely source of differences. There is some support for that conclusion here, as we find some of the most dramatic differences between the solutions in the GIN Seas region.

We can begin to understand the reduced sensitivity of the THC in the T31x3 configuration in the context of the results of Saenko et al. (2004). They show that more extensive ice coverage, as is the case in the T31x3 compared to the other configurations, reduces the sensitivity of the THC to transient climate forcing. They identify the decrease in melt water input in the deep-water formation region as a key mechanism for this dependence, with examples of increasing overturning with increasing CO_2 for experiments with unrealistically high sea ice area in the northern Atlantic. There is an indication of this type of behavior in the present experiments where the convective activity in the GIN Seas increases slightly with increasing CO_2 (Fig. 11), though the maximum overturning still decreases in our simulation. We note that this factor may contribute to the (smaller) difference in the response of the two higher-resolution experiments since the ice coverage decreases between the T42x1 and T85x1 configurations as well (Holland et al. 2006).

Previous studies have used different approaches to determining the relative roles of surface heat and freshwater fluxes to changes in the THC under global warming scenarios. Dixon et al. (1999) and Mikolajewicz and Voss (2000) conduct additional experiments replacing individual ocean–atmosphere flux fields in transient forcing experiments with their counterparts from a control integration. Latif et al. (2000) and Thorpe et al. (2001) take a diagnostic approach, examining balances within a single transient experiment. All of these studies, except that of Dixon et al. (1999), find that surface heat flux changes dominate the response of the THC, though to varying degrees. In this study we have followed the latter approach but use a different diagnostic methodology than has been considered previously in studies of the response of the THC to global warming: the water-mass transformation function. This diagnostic segregates surface forcing changes according to the density class that they act upon. We find that both differences in the mean overturning strength of the control experiments and the response of the overturning to transient forcing are well predicted by differences in the water-mass transformation rate. Additionally, the analysis shows that for all three configurations the decrease in the THC is driven by decreases in density due to changes in surface heat flux, consistent with the studies cited above. The contribution of changes in surface freshwater fluxes on those density classes involved in deep-water formation is to stabilize the THC. Similar to the studies of Thorpe et al. (2001) and Latif et al. (2000), we find that advective feedbacks, the reduction of poleward heat transport, and enhancement of poleward salt transport also act to maintain higher subpolar densities and stabilize the THC to transient climate forcing.

Wood et al. (1999) noted a substantial change in the structure of the circulation of the deep subpolar gyre in response to global warming, with the deep western boundary current bypassing the Labrador Basin at the time of quadrupling of CO_2. In these experiments, with the aid of the ideal age tracer, we see a substantial change in the pattern of ventilation, but not as dramatic of a shift in the circulation itself. Even in the T31x3 configuration with a weak overflow, there is still a clear

cyclonic deep circulation in the subpolar gyre, including the Labrador Basin, at the time of quadrupling of CO_2

5. Conclusions

In response to a 1% per year increase in CO_2, the strength of the Atlantic overturning circulation in three configurations of CCSM3 declines at a rate of 22%–26% of the corresponding control experiment maximum overturning per century. The mean meridional overturning and its variability on decadal time scales in the control experiments, the absolute rate of decrease in the transient forcing experiments, and the rate of recovery in periods of CO_2 stabilization all increase with increasing resolution. The T31x3 configuration has stronger quantitative and qualitative differences in the response relative to the T42x1 or T85x1 configurations than the latter two do to one another. As an example, the THC strength begins to recover following stabilization of CO_2 for the T85x1 and T42x1 configurations but continues to decline with CO_2 stabilized at quadruple present-day concentration in the T31x3 configuration. This brings the role of model resolution into focus when considering the applicability of studies of bifurcations of the climate system conducted with very coarse resolution ocean models, and suggests that further investigations of the response and recovery of the THC at even higher ocean model resolution are warranted to resolve these issues of resolution dependence.

The changes in high-latitude surface density are largest around the periphery of the subpolar gyre, associated with a poleward retreat of sea ice and alterations in the freshwater inputs due to melting. The change in density in deep-water formation regions is far less, reflecting the compensation of surface warming by increasing salinity, but still sufficient to cause a reduction in the depth of winter mixing. By examining the changes in ocean surface forcing with increasing CO_2 in the framework of the water-mass transformation function, we show that the decline in the overturning is driven by decreasing density of surface waters in the western subpolar North Atlantic due to increasing surface heat fluxes. The net effect of changes in surface freshwater fluxes on the highest density waters of the subpolar North Atlantic is to increase their density, that is, to stabilize the overturning circulation. It should be noted, however, that the CCSM3 has no representation of calving of glaciers that could potentially result in long-range transport of freshwater melt to the areas of deep-water formation via icebergs. Advective feedbacks, the reduction of meridional heat transport, and the enhancement of meridional salt transport from middle to high latitudes also act to stabilize the overturning circulation in our experiments.

Analysis of the trends in an ideal age tracer provide a direct measure of changes in ocean ventilation time scale in response to increasing CO_2. In the subpolar North Atlantic south of the Greenland–Scotland ridge system and throughout the basin below 2000 m, there is a significant increase in subsurface ages as open ocean deep convection is diminished and the THC weakens. At intermediate depths of the subpolar gyre, the dominant mode of ventilation switches from open ocean deep convection to overflows from the GIN Seas. In middle and low latitudes there is a decrease in age with increasing CO_2 for fixed depths within and just below the thermocline resulting from a decrease in the upwelling of old deep waters. In contrast, on fixed isopycnal surfaces within the thermocline, age increases with increasing CO_2 due to the descent of isopycnals as the ocean warms and deep upwelling declines. There is minimal change in the age of waters in the upper thermocline of the subtropics, consistent with the modest change in water-mass transformation rates for those density classes. The slowing of the THC and the lower ventilation of the North Atlantic will lead to a reduction in the rate of oceanic uptake of CO_2.

Acknowledgments. We thank Peter Gent for helpful discussions on this manuscript, and Keith Lindsay, Scott Weese, and Lawrence Buja for assistance in the configuration, integration, and analysis of the experiments. This study is based on model integrations that were performed by NCAR and CRIEPI with support and facilities provided by NSF, DOE, MEXT, and ESC/JAMSTEC.

REFERENCES

Bitz, C. M., P. R. Gent, R. A. Woodgate, M. M. Holland, and R. Lindsay, 2006: The influence of sea ice on ocean heat uptake in response to increasing CO_2. *J. Climate,* **19,** 2437–2450.

Bleck, R., and S. Sun, 2004: Diagnostics of the thermohaline circulation in a coupled climate model. *Global Planet. Change,* **40,** 233–248.

Broecker, W. S., 1997: Thermohaline circulation, the Achilles heel of our climate system: Will man-made CO_2 upset the current balance? *Science,* **278,** 1582–1588.

Collins, W. D., and Coauthors, 2006a: The Community Climate System Model version 3 (CCSM3). *J. Climate,* **19,** 2122–2143.

——, and Coauthors, 2006b: The formulation and atmospheric simulation of the Communty Atmosphere Model version 3 (CAM3). *J. Climate,* **19,** 2144–2161.

Cubasch, U., and Coauthors, 2001: Projections of future climate change. *Climate Change 2001: The Scientific Basis,* J. T. Houghton et al., Eds., Cambridge University Press, 525–582.

Dickinson, R. E., K. W. Oleson, G. Bonan, F. Hoffman, P. Thornton, M. Vertenstein, Z.-L. Zhang, and X. Zeng, 2006: The Community Land Model and its climate statistics as a component of the Community Climate System Model. *J. Climate,* **19,** 2302–2324.

Dickson, R. R., and J. Brown, 1994: The production of North Atlantic Deep Water: Sources, rates, and pathways. *J. Geophys. Res.,* **99** (C6), 12 319–12 341.

Dixon, K. W., T. L. Delworth, M. J. Spelman, and R. J. Stouffer, 1999: The influence of transient surface fluxes on the North Atlantic overturning in a coupled GCM climate change experiment. *Geophys. Res. Lett.,* **26,** 2749–2752.

Doney, S. C., W. G. Large, and F. O. Bryan, 1998: Surface ocean fluxes and water-mass transformation rates in the coupled NCAR Climate System Model. *J. Climate,* **11,** 1420–1441.

Gent, P. R., 2001: Will the North Atlantic Ocean thermohaline circulation weaken during the 21st century? *Geophys. Res. Lett.,* **28,** 1023–1026.

——, and G. Danabasoglu, 2004: Heat uptake and the thermohaline circulation in the Community Climate System Model, version 2. *J. Climate,* **17,** 4058–4069.

Hack, J. J., J. Caron, G. Danabasoglu, K. Oleson, C. Bitz, and J. E. Truesdale, 2006: CCSM3–CAM3 climate simulation sensitivity to changes in horizontal resolution. *J. Climate,* **19,** 2267–2289.

Holland, M. M., C. M. Bitz, E. C. Hunke, W. H. Lipscomb, and J. L. Schramm, 2006: Influence of the sea ice thickness distribution on polar climate in CCSM3. *J. Climate,* **19,** 2398–2414.

Hu, A., G. A. Meehl, and W. Han, 2004: Detecting thermohaline circulation changes from ocean properties in a coupled model. *Geophys. Res. Lett.,* **31,** L13204, doi:10.1029/2004GL020218.

Kiehl, J. T., and P. R. Gent, 2004: The Community Climate System Model, version 2. *J. Climate,* **17,** 3666–3682.

——, C. A. Shields, J. J. Hack, and W. Collins, 2006: The climate sensitivity of the Community Climate System Model: CCSM3. *J. Climate,* **19,** 2584–2596.

Large, W. G., and G. Danabasoglu, 2006: Attribution and impacts of upper-ocean biases in CCSM3. *J. Climate,* **19,** 2325–2346.

Latif, M., E. Roecknet, U. Mikolajewicz, and R. Voss, 2000: Tropical stabilizations of the thermohaline circulation in a greenhouse warming simulation. *J. Climate,* **13,** 1809–1813.

Manabe, S., and R. J. Stouffer, 1994: Multiple-century response of a coupled ocean–atmosphere model to an increase of atmospheric carbon dioxide. *J. Climate,* **7,** 5–23.

Mikolajewicz, U., and R. Voss, 2000: The role of individual air-sea flux components in CO_2-induced changes of the ocean's circulation and climate. *Climate Dyn.,* **16,** 627–642.

Raper, S. C. B., J. M. Gregory, and R. J. Stouffer, 2002: The role of climate sensitivity and ocean heat uptake on AOGCM transient temperature response. *J. Climate,* **15,** 124–130.

Saenko, O. A., M. Eby, and A. J. Weaver, 2004: The effect of sea-ice extent in the North Atlantic on the stability of the thermohaline circulation in global warming experiments. *Climate Dyn.,* **22,** 689–699.

Sarmiento, J. L., and N. Gruber, 2002: Sinks for anthropogenic carbon. *Phys. Today,* **55,** 30–36.

——, T. M. Hughes, R. J. Stouffer, and S. Manabe, 1998: Simulated response of the ocean carbon cycle to anthropogenic climate warming. *Nature,* **393,** 245–249.

Schweckendiek, U., and J. Willebrand, 2005: Mechanisms affecting the overturning response in global warming simulations. *J. Climate,* **18,** 4925–4936.

Smith, R., and P. Gent, 2004: Reference manual for the Parallel Ocean Program (POP): Ocean component of the Community Climate System Model (CCSM2.0 and 3.0). Tech. Rep. LAUR-02-2484, Los Alamos National Laboratory, Los Alamos, NM, 75 pp. [Available online at http://www.ccsm.ucar.edu/models/ccsm3.0/pop/doc/manual.pdf.]

Speer, K., and E. Tziperman, 1992: Rates of water mass formation in the North Atlantic Ocean. *J. Phys. Oceanogr.,* **22,** 93–110.

Steele, M., R. Morely, and W. Ermold, 2001: PHC: A global hydrography with a high-quality Arctic Ocean. *J. Climate,* **14,** 2079–2087.

Stocker, T. F., and A. Schmittner, 1997: Influence of CO_2 emissions rates on the stability of the thermohaline circulation. *Nature,* **388,** 862–865.

Thiele, G., and J. L. Sarmiento, 1990: Tracer dating and ocean ventilation. *J. Geophys. Res.,* **95** (C6), 9377–9391.

Thorpe, R. B., J. M. Gregory, T. C. Johns, R. A. Wood, and J. F. B. Mitchell, 2001: Mechanisms determining the Atlantic thermohaline circulation response to greenhouse gas forcing in a non-flux-adjusted coupled climate model. *J. Climate,* **14,** 3102–3116.

Wood, R. A., A. Keen, J. Mitchell, and J. Gregory, 1999: Changing spatial structure of the thermohaline circulation in response to atmospheric CO_2 forcing in a climate model. *Nature,* **399,** 572–575.

——, M. Velinga, and R. Thorpe, 2003: Global warming and thermohaline circulation stability. *Philos. Trans. Roy. Soc. London,* **361A,** 1961–1975.

Yeager, S., C. Shields, W. G. Large, and J. J. Hack, 2006: The low-resolution CCSM3. *J. Climate,* **19,** 2545–2566.